Research Article | Open Access

Nanomedicine Therapeutics

Anaki *et al. Nanomed Ther.* 2026;1:4 **DOI:**10.20517/nmt.2026.03

Bispecific gold nanoparticles enhance therapeutic efficacy in HER2-positive breast cancer

Adi Anaki[1], Chen Tzror-Azankot[1], Ulugbek Saidvaliev[2], Oshra Betzer[3], Ayelet Zafran[3], Menachem Motiei[1], Tamar Sadan[1], Dror Fixler[2], Rachela Popovtzer[1]

Keywords:
Gold nanoparticles, bispecific, anti-HER2 antibodies, trastuzumab, pertuzumab, cancer therapy

Citation: Anaki A, Tzror-Azankot C, Saidvaliev U, Betzer O, Zafran A, Motiei M, Sadan T, Fixler D, Popovtzer R. Bispecific gold nanoparticles enhance therapeutic efficacy in HER2-positive breast cancer. *Nanomed Ther.* 2026;1:4. https://dx.doi.org/10.20517/nmt.2026.03

Received: 11 Jun 2026
First Decision: 17 Jul 2026
Revised: 21 Aug 2026
Accepted: 26 Aug 2026
Published: 3 Sep 2026

Academic Editor:
Xiangyang Shi
Copy Editor:
Shu-Yuan Duan
Production Editor:
Shu-Yuan Duan

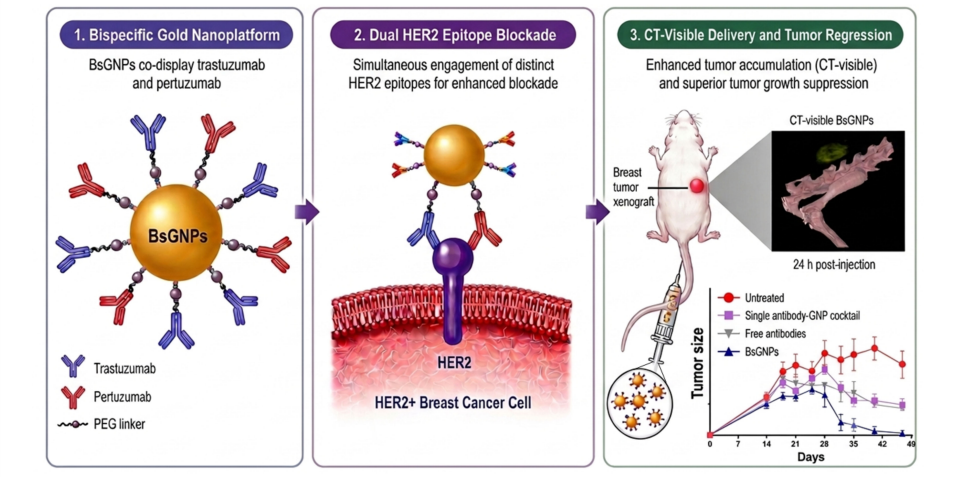

Abstract

Bispecific antibodies provide a powerful strategy for cancer therapy by enabling simultaneous engagement of multiple tumor-associated epitopes. However, their clinical translation in solid tumors is limited by various challenges, including complex engineering and poor intratumoral penetration. Here, we present a nanotechnology-based alternative by designing bispecific gold nanoparticles (BsGNPs) that co-display the clinically approved anti-HER2 antibodies trastuzumab and pertuzumab on a single nanoparticle platform. In HER2-overexpressing breast cancer cell lines, BsGNPs induced significantly higher antiproliferative activity compared with free antibodies or a cocktail of single-antibody-conjugated GNPs. In a HER2-positive BT-474 xenograft model, *in vivo* computed tomography imaging demonstrated efficient intratumoral accumulation of BsGNPs. Moreover, BsGNPs produced pronounced and sustained tumor regression, significantly outperforming both free antibodies and the cocktail of single-antibody GNPs. These results show that presenting two antibody types on a single nanoparticle can enhance therapeutic efficacy in solid tumors. Thus, BsGNPs offer a modular, theranostic platform with potential to advance nanomedicine-based cancer therapy.

[1]Faculty of Engineering and the Institute of Nanotechnology & Advanced Materials, Bar-Ilan University, Ramat Gan 5290002, Israel.
[2]Faculty of Engineering, Department of Biomedical Engineering, Jan Koum Center for Nanoscience and Nanotechnology, Light Matter Interaction Center, Tel Aviv University, Tel Aviv 69978, Israel.
[3]Nanocarry Therapeutics Ltd., Kadima-Tzoran 4282300, Israel.

Correspondence to: Prof. Rachela Popovtzer, Faculty of Engineering and the Institute of Nanotechnology & Advanced Materials, Bar-Ilan University, Ramat Gan 5290002, Israel. E-mail: rachela.popovtzer@biu.ac.il

INTRODUCTION

Bispecific antibodies represent a growing modality in cancer therapy, as their ability to simultaneously engage two distinct antigens or epitopes enables therapeutic mechanisms beyond those of monospecific antibodies[1]. This dual-targeting capability facilitates mechanisms such as enhanced receptor blockade, immune cell recruitment, and synergistic pathway inhibition[1]. To date, numerous bispecific antibodies have entered clinical development, with notable success in hematologic malignancies[2]. However, their broader clinical translation, particularly to solid tumors, remains challenging due to design complexity and biological barriers to delivery[3]. The complex molecular architecture of bispecific antibodies necessitates correct heavy- and light-chain pairing, preservation of dual binding affinity, and maintenance of stability. These constraints pose substantial engineering challenges[4,5], often resulting in aggregation and reduced yield[6]. In solid tumors, poor tissue penetration and the heterogeneous distribution of antibodies often limit efficacy[7-12]. Although smaller bispecific antibody fragments may improve tumor penetration, they typically exhibit rapid clearance and limited therapeutic durability[13].

Nanotechnology offers a versatile strategy for addressing these limitations. Nanoparticle-based systems provide modular platforms whose physicochemical and surface properties can be tailored to modulate tumor accumulation, tissue penetration, and intratumoral distribution[14]. Preclinical and clinical studies have demonstrated enhanced tumor accumulation of nanoparticle formulations relative to free therapeutics, mediated by both passive and active transport mechanisms[14-16]. Furthermore, nanoparticle surfaces support the co-conjugation of distinct intact antibodies, allowing multiple targeting specificities to be incorporated into a single carrier without the need for recombinant antibody engineering[17-20].

Among nanoplatforms, gold nanoparticles (GNPs) are particularly attractive for application in bispecific targeting because of their biocompatibility, tunable size, and straightforward surface modification[21-24]. These properties facilitate the controlled conjugation of intact antibodies while preserving antigen-binding affinity and biological activity[21,22]. The high X-ray attenuation of gold also allows GNPs to serve as computed tomography (CT) contrast agents, supporting noninvasive visualization and *in vivo* tracking of nanoparticle-based therapeutics[25-28].

Here, we report the development of bispecific gold nanoparticles (BsGNPs) that co-display trastuzumab and pertuzumab on a single nanoplatform. These antibodies bind distinct HER2 epitopes and exert complementary mechanisms of receptor inhibition[29]. Dual HER2 blockade with free trastuzumab and pertuzumab is a clinically established treatment strategy for HER2-positive breast cancer[30,31]. In parallel, several recombinant bispecific formats designed to target non-overlapping epitopes of HER2 are undergoing clinical investigation[3,32-35]. Nonetheless, free-antibody combination regimens and recombinant bispecific constructs face inherent limitations in delivery, molecular design, or both.

We investigated whether nanoparticle-mediated co-presentation of the two antibodies could improve therapeutic efficacy in HER2-positive breast cancer models. BsGNPs exhibited superior antiproliferative activity *in vitro* and induced pronounced tumor regression *in vivo*, compared with free antibodies or a cocktail of single-antibody-conjugated nanoparticles. Our findings suggest BsGNPs as a modular strategy to enhance HER2-targeted therapy while addressing key limitations of bispecific antibody approaches in solid tumors.

MATERIALS AND METHODS

BsGNP synthesis and characterization

Synthesis of ~ 20 nm spherical GNPs was performed using sodium citrate (Sigma Aldrich, MO, USA) as a reducing agent, following the methodology established by Enustun and Turkevich[36]. A 414 µL aliquot of a 50% w/V $HAuCl_4$ solution was added to 200 mL of purified water (Hylabs, Rehovot, Israel), and the mixture was brought to a boil in a paraffin oil bath. Subsequently, 4.05 mL of a 10% sodium citrate solution was introduced, and the solution was stirred for 5 min. After cooling to room temperature, the GNP suspension (~ 204 mL) was functionalized with a thiol-polyethylene-glycol (PEG) layer using 9.7 µmol total thiolated PEG. The PEG layer comprised 60 mol% mPEG-SH (Mw ≈ 6 kDa; Cat #729159, Sigma Aldrich), 20 mol% heterofunctional thiol-PEG-carboxylic acid (SH-PEG-COOH) of Mw

≈ 5 kDa (Cat #757845, Sigma Aldrich) conjugated to insulin (100 IU), and 20 mol% SH-PEG-COOH Mw ≈ 3.5 kDa (Cat #757837, Sigma Aldrich) for conjugation of the antibodies, namely, trastuzumab and/or pertuzumab (Roche Ltd, Basel, Switzerland), or non-specific human immunoglobulin G (IgG)-1 isotype control antibody (InVivoMAb, cat# BE0297; Bio X Cell, Lebanon, NH, USA). After PEG addition, the suspension was stirred for 2 h; the PEG-coated GNPs were then centrifuged at 20,000 rpm for 20 min, the supernatant was removed, and the pellet was resuspended in purified water. This centrifugation and resuspension procedure was repeated three times. For conjugation, PEG carboxyl groups were first activated for 30 min using 1-ethyl-3-(3-(dimethylamino)propyl) carbodiimide HCl (EDC; Cat #22980, Thermo Fisher Scientific, Waltham, MA, USA) and N-hydroxy-sulfo-succinimide sodium salt (Sulfo-NHS; Cat# 24510, Thermo Fisher Scientific). For this purpose, fresh 30 mg/mL stock solutions of EDC and Sulfo-NHS were prepared immediately before use and added to achieve final concentrations of 1 mM each in the activation reaction. Activation was performed at pH 6.5. Excess EDC/NHS was removed by centrifugation (13,000 rpm, 30 min) and the solvent was washed and replaced with PBS (Hylabs). For nanoparticle formulations used in the *in vitro* experiments (IgG-GNPs, trastuzumab-GNPs, pertuzumab-GNPs, and BsGNPs), antibodies were added at a total amount of 5 mg per formulation. For formulations intended for the *in vivo* experiments (trastuzumab-GNPs, pertuzumab-GNPs, and BsGNPs), the antibody input was increased to 10 mg per formulation to achieve a higher antibody loading required for *in vivo* dosing. For BsGNPs, trastuzumab and pertuzumab were added at a mass ratio of 2:1 in both preparations. GNPs were incubated with the antibodies for 3 h, then centrifuged (13,000 rpm, 30 min), and the antibody-conjugated GNP pellet was separated from the reaction supernatant. The final GNP concentration was 30 mg/mL as determined by inductively coupled plasma optical emission spectrometry (ICP-OES).

The nanoparticles were characterized using transmission electron microscopy (TEM; JEM-1400, JEOL, Tokyo, Japan) to assess their size and shape. Additional characterization was performed through ultraviolet-visible spectroscopy (UV-Vis; UV-1650 PC, Shimadzu Corp., Kyoto, Japan), dynamic light scattering (DLS; NANO-flex, Particle Matrix, Germany), and zeta potential measurements (ZetaSizer 3000HS, Malvern Instruments, Malvern, UK) following each stage of coating. HER2 binding by BsGNPs was assessed by enzyme-linked immunosorbent assay (ELISA) using recombinant human HER2-Fc-coated plates (Cat# HE2-H5253; ACROBiosystems, Newark, DE, USA) at 0.05 μg/well overnight at 4 °C and blocked with 2% BSA. After incubation with BsGNPs (1 h at 37 °C) followed by horseradish peroxidase-conjugated goat anti-human IgG (Jackson ImmunoResearch, West Grove, PA, USA) (1:20,000) for 1 h at 37 °C, binding was detected with 3,3',5,5′-tetramethylbenzidine (TMB; Surmodics, Horsham, PA, USA), and absorbance was measured at 640 nm after blank subtraction. Antibody loading was assessed using NanoDrop spectrophotometry (NanoDrop™ 2000/2000c, Thermo Scientific, Waltham, MA, USA) by measuring unbound antibody concentration in the supernatant after BsGNP purification, and conjugated antibody was determined by mass balance.

Dual antibody fluorescence labeling of gold nanoparticles

Trastuzumab was biotinylated using EZ-Link Sulfo-NHS-LC-Biotin (Cat# 21335, Thermo Fisher Scientific) according to the manufacturer's protocol, followed by dialysis against PBS (Slide-A-Lyzer MINI, 50-100 kDa MWCO). The biotinylated antibody was subsequently conjugated to streptavidin-phycoerythrin (PE) at a 1:1 molar ratio for 30 min at room temperature in the dark. Pertuzumab was fluorescently labeled with NHS-Fluorescein (Cat# 46410, Thermo Fisher Scientific) by incubation at a 100:1 molar ratio (dye:antibody) for 2 h at room temperature, protected from light. Excess unbound dye or PE was removed by several centrifugal filtration repeats (Amicon Ultra, 50 kDa MWCO). The resulting fluorescent antibody conjugates were stored at 4 °C in the dark until use. Fluorescently labeled antibodies (trastuzumab-phycoerythrin and pertuzumab-fluorescein) were incubated with activated PEGylated GNPs for 3 h at room temperature under gentle agitation, resulting in three types of conjugates: GNPs bearing only trastuzumab-PE, only pertuzumab-fluorescein, or both antibodies simultaneously. Conjugates were purified by centrifugation (14,000 rpm, 20 min) and resuspended in PBS. The dual-labeled antibody-GNP conjugates were stored at 4 °C in the dark until further analysis. Fluorescence

intensity was measured using a Synergy H1 multi-mode microplate reader (Agilent, Santa Clara, CA, USA).

Fluorescence lifetime imaging microscopy of BsGNPs

The fluorescence lifetime imaging microscopy (FLIM) setup consisted of a Lambert Instruments system (LIFA, Groningen, The Netherlands), frequency-domain (FD) FLIM, with the excitation source of a multi-light-emitting diode (LED) working in 468 nm wavelength mode, modulated in a sinusoidal mode by a signal generator (Prior OptiScan I, Rockland, Massachusetts, United States) and a time-resolved intensified low-light imaging CMOS camera with ultra-short gating. In this experiment, three scanning-mode frequencies (34 MHz, 38 MHz, and 42 MHz) were used to excite the samples. An Olympus IX-81 model inverted microscope with a 10× NA¼ 0.4 objective (Olympus, Tokyo, Japan) was used to achieve precise focusing on the samples. Samples were prepared on glass slides by taking 5 ml of each solution onto separate slides using a pipette. Each slide was then placed under the microscope and analyzed using LIFA FD-FLIM software. Average and standard deviation values were estimated using LIFA FLIM v1.2.26 software (Lambert Instruments).

Cell culture

Human breast cancer SKBR3 cells (ATCC Cat# HTB-30, RRID: CVCL_0033), human breast cancer BT-474 cells (ATCC, Cat# HTB-20, RRID: CVCL_0179), or epidermoid carcinoma A431 cells (ATCC, Cat# CRL-1555, RRID: CVCL_0037) were cultured in Dulbecco's modified Eagle's medium (DMEM; Sigma-Aldrich) supplemented with 10% fetal bovine serum (FBS, Cat# 04-001-1A, Biological Industries, Beit HaEmek, Israel), 2 mM L-Glutamine, and 1% Penicillin/Streptomycin (Biological Industries, Beit HaEmek, Israel). HepG2 human hepatocellular carcinoma cells (ATCC, cat# HB-8065, RRID CVCL_0027) were maintained in RPMI 1640 (#SH30096.01, HyClone, Wilmington, USA) supplemented with 10% FBS, 2 mM L-glutamine, 100 U/mL penicillin, and 100 µg/mL streptomycin; viability assays were performed in the corresponding antibiotic-free medium. KUP5 cells (mouse Kupffer cell line clone 5) (RIKEN BRC, cat# RCB4627, RRID CVCL_6C88) were cultured in high-glucose DMEM (#11995-065, Gibco, USA) supplemented with 10% FBS, 10 µg/mL human insulin, and 250 µM monothioglycerol (Sigma-Aldrich). Cells were maintained at 37 °C under humidified conditions with 5% CO_2. All cell lines were used between passages 3 and 6 post-thaw. The absence of mycoplasma contamination in all cell lines was confirmed prior to experimental use by Myco-One Step Mycoplasma Detector (Cat# D201-02, Vazyme Biotech, Nanjing, China).

Cell proliferation and viability assays

For proliferation assays, cells were counted using a hemocytometer and seeded at 1×10^4 cells/well in 96-well plates under normal growth conditions. After 24 h, cells were treated with BsGNPs or IgG-GNPs (0.3, 0.6, 1.5, or 3 µg/mL of bound antibody corresponding to gold concentrations of 10, 20, 50, or 100 µg/mL), 3 µg/ml total free antibodies, or the single-antibody-GNP cocktail (trastuzumab-GNPs and pertuzumab-GNPs; 3 µg/ml of bound antibody). Antibody-equivalent concentrations were determined based on the measured antibody loading per GNP. Treatments were diluted in culture medium to the indicated concentrations, with a final volume of 200 µL per well (three technical replicates per condition). Cells were maintained under standard culture conditions for 6 days; on day 4, medium was replaced, and treatments were replenished at the same concentrations. Experimental data comprised 3-4 biological replicates performed on different days with three technical replicates per biological replicate. Technical replicates were averaged within each independent experiment. Cell proliferation was assessed using the CyQUANT™ NF Cell Proliferation Assay kit (#C35006, Thermo Fisher Scientific, Waltham, MA, USA), following the manufacturer's protocol. For viability testing, HepG2 or KUP5 cells were seeded (5×10^5 cells/mL); 24 h later, cells were incubated with the BsGNPs in triplicate for 48 h. Cell viability was quantified using the MTT reduction assay [3-(4,5-dimethylthiazol-2-yl)-2,5-diphenyltetrazolium bromide; Sigma-Aldrich, M5655].

BT-474 tumor model and treatment

A BT-474 breast cancer tumor model was established by subcutaneous injection of 5×10^6 BT-474 cells into the back flank of 6-week-old Hsd:Athymic nude-Foxn1nu female mice (Harlan Laboratories, Jerusalem, Israel). Once the tumors reached 40 mm^2 (day 14), mice were randomly divided into groups and received weekly IP injections of either free anti-

bodies, a cocktail of single-antibody GNPs (trastuzumab-GNPs and pertuzumab-GNPs), or BsGNPs. All treatments were administered at an equivalent antibody dose (free or bound) of 0.945 mg per mouse per injection (with 12.6 mg Au/injection administered in the GNP-treated groups). Treatments were given on days 14, 21, 28, and 35. Tumor growth was monitored in a blinded manner at several time points over the study. Tumor length and width were measured using a caliper, and tumor area was calculated as length × width (mm^2). At the end of the experiment, the mice underwent CT imaging to evaluate gold accumulation within the tumor. Following euthanasia, tissue samples were collected to assess the biodistribution of gold in various organs using ICP-OES.

CT imaging and analysis

At 24 h post-injection, CT scans were performed to assess nanoparticle distribution and tumor morphology. The abdominal (tumor) region was imaged using a Bruker Skyscan 1176 micro-CT scanner with a 35 μm nominal resolution, a 0.2 mm aluminum filter, and a tube voltage of 45 kV. Reconstruction was carried out using a modified Feldkamp algorithm with GPU acceleration via SkyScan NRecon software. Image processing included ring artifact reduction, Gaussian smoothing (3%), and beam hardening correction (20%). Volume-rendered 3D images were generated using RGBA transfer functions in SkyScan CT-Volume ("CT-Vol") and CT-Voxel ("CT-Vox") software.

Gold quantification in tumor and organs

At 24 h post-injection and following CT imaging, mice (n = 3) were sacrificed, tumors and major organs (liver, spleen, kidneys, lungs, and heart) were excised, and blood (~ 1.5 mL) was collected. The mean ± standard deviation (SD) weights of the major organs were 0.918 ± 0.036 g for the liver, 0.076 ± 0.011 g for the spleen, 0.218 ± 0.018 g for the kidneys, 0.222 ± 0.074 g for the lungs, and 0.112 ± 0.010 g for the heart. Tissues were digested in aqua regia (a mixture of nitric acid and hydrochloric acid at a 1:3 volume ratio) and diluted with purified water to a final volume of 5 mL. After filtration, gold concentrations in tumors and organs were quantified using inductively coupled plasma optical emission spectroscopy (ICP-OES; 710, Agilent Technologies) with calibration curves prepared from standard gold solutions (0, 0.1, 0.5, 1, 5, and 10 mg/L). Percentage of injected dose (%ID) was determined by calculation of ICP-OES measured gold concentration (ppm) × final sample volume (mL) / total amount of injected gold (mg) × 100.

Blood chemistry analysis

Blood samples collected for serum chemistry analysis were allowed to clot for 30 min at room temperature and centrifuged at 3,000 × g for 10 min at 22 °C. Serum creatinine, urea, alanine aminotransferase (ALT), aspartate aminotransferase (AST), and alkaline phosphatase (ALP) levels were measured using an automatic biochemistry analyzer (Roche Cobas c311) with commercial assay kits (Cat# 03263991190, 04460715190, 20764957322, 20764949322, and 03333701190; Roche Diagnostics, Basel, Switzerland) according to the manufacturer's instructions.

Animal care

All animals were housed under controlled conditions, maintaining a 12:12 h light/dark cycle, a stable temperature of 23 °C, and 50% humidity, with unrestricted access to food and water. All animal procedures were conducted at the Animal Research Center of Bar-Ilan University in accordance with the guidelines and regulations of the National Institutes of Health (DHEW Pub. No. NIH 78-23). The Bar-Ilan University Institutional Animal Care and Use Committee approved the study protocol, and the study was conducted under its supervision (protocol no. 2401-104-5).

Statistical analysis

Statistical analysis was conducted using GraphPad Prism 10 (GraphPad Software, Inc.). Two-tailed paired Student's t-tests were used for paired two-group comparisons. For *in vitro* experiments, one-way analysis of variance (ANOVA) with Tukey's multiple-comparison test or two-way ANOVA with Holm-Šídák's multiple-comparisons test was used for independent-group analyses, with biological replicates as the experimental units. Longitudinal tumor-size data were analyzed using two-way ANOVA with repeated measurements followed by Tukey's multiple-comparisons test. Parametric analyses assumed approximately Gaussian residuals (formal normality testing was not performed because of the small sample sizes). Homogeneity of variance was assessed, where applicable, using the Brown-Forsythe test. A P-value of < 0.05 was consid-

ered statistically significant.

RESULTS

Synthesis and physicochemical characterization of BsGNPs

Gold nanoparticles were synthesized and subsequently functionalized with PEG linkers to which trastuzumab and pertuzumab were covalently attached. Transmission electron microscopy confirmed a uniform, spherical morphology with an average core diameter of 20.0 ± 3.4 nm and 20.0 ± 3.1 nm for bare nanoparticles and BsGNPs, respectively [Figure 1A]. We previously showed that this size optimally balances tumor delivery and CT imaging capability[22]. UV-visible spectroscopy revealed stepwise red-shifts in the surface plasmon resonance following PEGylation and antibody conjugation [Figure 1B], consistent with progressive surface modification. Dynamic light scattering measurements showed an increase in hydrodynamic diameter from 25 ± 3 nm for bare GNPs to 65 ± 8 nm for BsGNPs [polydispersity Index (PDI) = 0.1878; Figure 1C], and zeta potential values shifted from -39.8 mV to -13.7 ± 9 mV after antibody conjugation [Figure 1D]. Together, these size and surface charge changes confirmed successful antibody conjugation. These physicochemical parameters remained comparable after three months of storage at 4 °C (hydrodynamic diameter, 60 ± 7 nm; PDI 0.1944; zeta potential, -14.0 ± 6.4 mV). In addition, ELISA showed that HER2-binding activity was maintained over one week at 4 °C storage (EC50 of 0.134 ± 0.084 μg/mL after synthesis and 0.118 ± 0.058 μg/mL after a week; mean ± SD, n = 3 independent samples; two-tailed paired Student's t-test, P = 0.62). These data support the physicochemical stability of BsGNPs and retention of their binding functionality. NanoDrop-based analysis indicated an antibody loading of 9.9 ± 2.0 antibodies per BsGNP for the preparations used in the *in vitro* experiments. To achieve higher antibody loading required for *in vivo* dosing, the *in vivo* preparations were synthesized with increased antibody input, yielding an average of 24.7 ± 1.8 antibodies per BsGNP (mean ± SD, n = 3 independent samples).

To confirm that trastuzumab and pertuzumab are co-conjugated on the same nanoparticle, rather than distributed across separate, singly functionalized populations, two complementary BsGNP formulations were synthesized. In the first formulation, trastuzumab was labeled with phycoerythrin (PE) while pertuzumab remained unlabeled; in the second, pertuzumab was labeled with fluorescein (FLU) while trastuzumab remained unlabeled [Figure 2A]. This approach enabled independent verification of each antibody's incorporation into the BsGNPs while controlling potential cross-labeling artifacts. Fluorescence intensity analysis revealed clear and mutually exclusive signal detection in the expected channels [Figure 2B and C]: BsGNPs bearing PE-labeled trastuzumab exhibited strong fluorescence in the PE channel (MFI > 3×10^4) with negligible signal in the FLU channel, whereas BsGNPs bearing FLU-labeled pertuzumab showed the opposite pattern, with robust FLU fluorescence (MFI ~ 950) and minimal PE background. BsGNPs lacking fluorescent labels displayed negligible signal in both channels, confirming assay specificity. To confirm co-localization of both antibodies on individual nanoparticles, FLIM was performed on BsGNPs functionalized with either single-labeled or dual-labeled antibodies [Figure 2D]. All labeled samples exhibited discrete, punctate fluorescent signals corresponding to antibody-functionalized nanoparticles, whereas unlabeled BsGNPs showed no detectable fluorescence. Nanoparticles carrying only fluorescein- or PE-labeled antibodies displayed fluorescence lifetimes corresponding to the native lifetimes of the free dyes in solution (~ 4 ns for FLU and ~ 2 ns for PE; Figure 2E). In contrast, dual-labeled BsGNPs exhibited multicomponent fluorescence lifetimes spanning both characteristic lifetime ranges, which were detected within the same regions of interest, confirming the co-localization of both fluorophores and thus both antibodies, on individual nanoparticles [Figure 2E]. Collectively, these results demonstrate successful dual functionalization of trastuzumab and pertuzumab on the gold nanoparticle surface.

BsGNPs inhibit proliferation of HER2 breast cancer cells

The antiproliferative effects of BsGNPs were first evaluated *in vitro*. The HER2-overexpressing breast cancer cell line SKBR3 was treated with either BsGNPs or non-specific IgG-conjugated GNPs (IgG-GNPs) at increasing concentrations (0.3-3 μg/mL of bound antibody). IgG-GNPs showed no concentration-dependent reduction in cell proliferation, whereas BsGNPs progressively reduced proliferation with increasing concentration. At matched

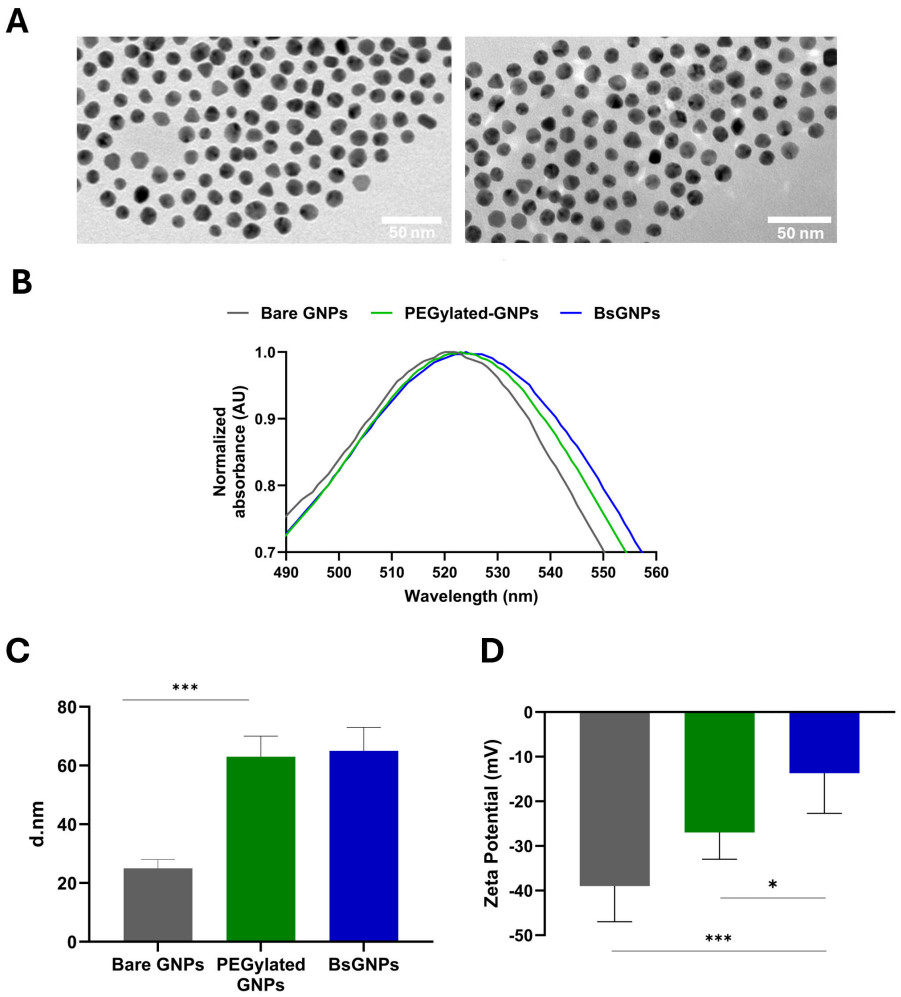

Figure 1. Physicochemical characterization of bispecific gold nanoparticles (BsGNPs). (A) Representative TEM images of bare GNPs (left) and BsGNPs (right) showing uniform, spherical morphology (scale bar = 50 nm); (B) Normalized UV-visible absorption spectra of bare GNPs, PEGylated GNPs, and BsGNPs, demonstrating characteristic red-shifts in the surface plasmon resonance following sequential surface functionalization; (C) Hydrodynamic diameters measured by dynamic light scattering (DLS) after each modification step, indicating increased particle size upon PEGylation and antibody conjugation. (D) Zeta potential measurements showing progressive modulation of surface charge during nanoparticle functionalization. In (C and D), data are presented as mean ± SD of three independent nanoparticle preparations analyzed by one-way ANOVA followed by Tukey's multiple-comparisons test; *$P < 0.05$, ***$P < 0.001$. GNP: gold nanoparticle; PEG: polyethylene-glycol; TEM: transmission electron microscopy; SD: Standard deviation; ANOVA: analysis of variance.

antibody concentrations, proliferation was significantly lower following BsGNP treatment than following IgG-GNP treatment at 0.6, 1.5, and 3 μg/mL ($P < 0.01$, $P < 0.001$, and $P < 0.0001$, respectively). Within the BsGNP group, 1.5 μg/mL significantly reduced proliferation compared with 0.3 μg/mL ($P < 0.05$), while 3 μg/mL significantly reduced proliferation compared with 0.3 and 0.6 μg/mL ($P < 0.0001$ and $P < 0.01$, respectively; two-way ANOVA with Holm-Šídák's multiple-comparisons test; Figure 3A). Next, using the most effective concentration, we compared BsGNP activity to an equivalent dose of free trastuzumab and pertuzumab or a cocktail of single-antibody GNPs consisting of trastuzumab-GNPs and pertuzumab-GNPs (total antibody concentration of 3 μg/mL per group). BsGNPs exhibited significantly greater antiproliferative activity than both the free antibody combination and the single-antibody GNP cocktail (trastuzumab-GNPs and pertuzumab-GNPs) ($P < 0.01$ and $P < 0.05$, respectively; Figure 3B).

We further evaluated BsGNP activity across cell lines with differing HER2 expression, including low-HER2-expressing human epidermoid carcinoma A431 cells[37,38] and the HER2-overexpressing human breast cancer BT-474 and SKBR3 cells[39,40]. BsGNPs significantly reduced cell proliferation in SKBR3

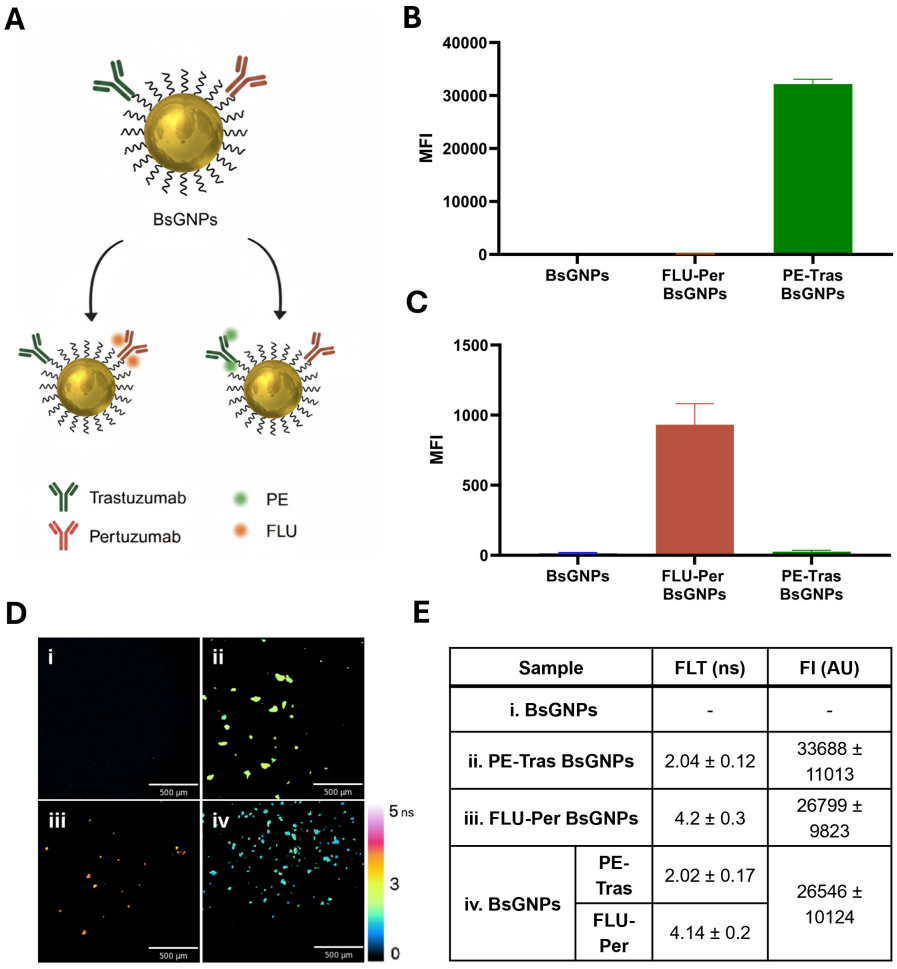

Sample		FLT (ns)	FI (AU)
i. BsGNPs		-	-
ii. PE-Tras BsGNPs		2.04 ± 0.12	33688 ± 11013
iii. FLU-Per BsGNPs		4.2 ± 0.3	26799 ± 9823
iv. BsGNPs	PE-Tras	2.02 ± 0.17	26546 ± 10124
	FLU-Per	4.14 ± 0.2	

Figure 2. Validation of dual antibody co-localization on BsGNPs. (A) Schematic illustrating the dual-preparation strategy to verify co-localization of trastuzumab and pertuzumab on the same gold nanoparticle. Two complementary BsGNP formulations were generated: one containing PE-labeled trastuzumab with unlabeled pertuzumab, and the other containing FLU-labeled pertuzumab with unlabeled trastuzumab; (B) Fluorescence intensity measured in the PE channel, showing a strong signal exclusively for BsGNPs bearing PE-labeled trastuzumab; (C) Fluorescence intensity measured in the FLU channel, showing a specific signal exclusively for BsGNPs bearing FLU-labeled pertuzumab. Unlabeled BsGNPs exhibit negligible signal in both channels (B and C); (D) Representative FLIM images of (i) unlabeled BsGNPs, (ii-iii) single-labeled BsGNPs (PE-labeled or FLU-labeled, respectively), and (iv) dual-labeled (FLU/PE) BsGNPs. Fluorescent puncta correspond to antibody-functionalized nanoparticles. Scale bar = 500 µm; color bar indicates fluorescence lifetime (ns). (E) Fluorescence lifetime (FLT) and fluorescence intensity (FI) analyses. Characteristic single-component lifetimes for singly-labeled BsGNPs and multicomponent lifetimes in dual-labeled BsGNPs were detected within the same regions of interest, confirming co-localization of both fluorophores and thus both antibodies on individual nanoparticles. ^{2} estimation criteria for all FLT values in our data analysis model were less than 15. Results are shown as the mean ± SD of three independently prepared samples (with the value for each sample calculated as the mean of five consecutive measurements). AU: Arbitrary units; ns: nanoseconds; BsGNP: bispecific gold nanoparticle; PE: phycoerythrin; FLU: fluorescein; SD: standard deviation.

cells compared with A431 cells ($P < 0.05$; Figure 3C). While the reduction observed in BT-474 cells did not reach statistical significance compared with A431 cells ($P = 0.0503$), BsGNP antiproliferative activity in BT-474 cells was not significantly different from that observed in SKBR3 cells [Figure 3C].

To investigate the cytotoxicity of the BsGNPs, we treated both human hepatocarcinoma cells (HepG2) and mouse Kupffer cells (KUP5) with increasing gold concentrations (10-100 µg/mL) for 48 h. MTT assay showed that BsGNPs did not affect cell viability in either cell type at any dose [Figure 3D].

Taken together, these findings demonstrate that BsGNPs induce an enhanced, dose-dependent antiproliferative effect in HER2-expressing cells, outperforming both the free antibody combination and the single-antibody nanoparticle cocktail. The findings also suggest an antiproliferative effect that

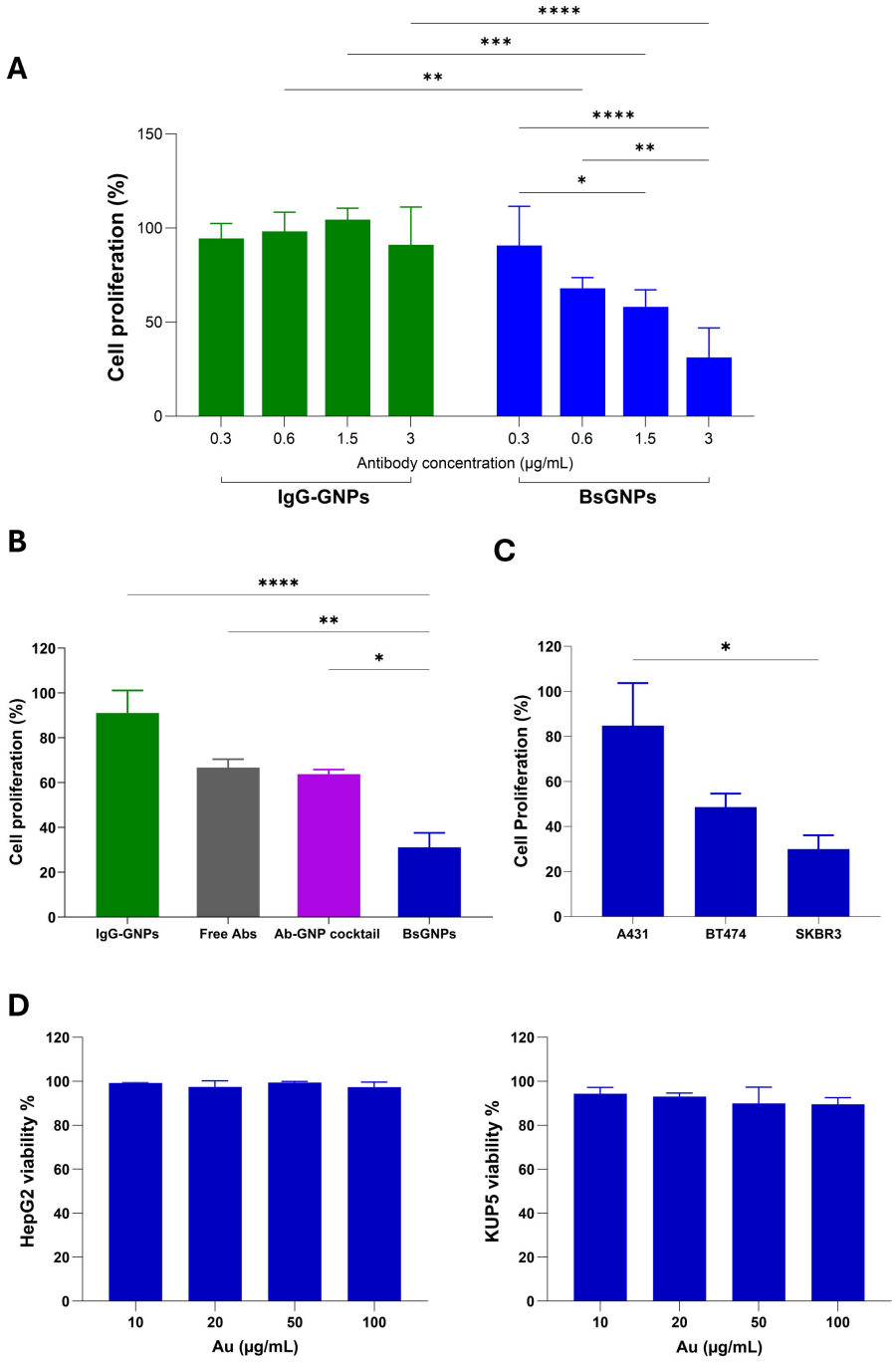

Figure 3. *In vitro* antiproliferative activity and cytotoxicity of BsGNPs. (A) SKBR3 cells were incubated with IgG-GNPs or BsGNPs at increasing concentrations (0.3, 0.6, 1.5, or 3 μg/ml of bound antibody) for 6 days; proliferation was normalized to untreated controls (100%). Statistical significance was assessed by two-way ANOVA followed by Holm-Šídák's multiple-comparisons test. Significance was seen between BsGNPs and IgG-GNPs at matched concentrations of 0.6, 1.5, and 3 μg/mL, and within the BsGNP group between 0.3 and 1.5 μg/mL, 0.3 and 3 μg/mL, and 0.6 and 3 μg/mL. *$P < 0.05$, ** $P < 0.01$, *** $P < 0.001$, **** $P < 0.0001$. Mean ± SD, $n = 4$ biological replicates; $n = 3$ technical replicates per biological replicate; (B) Cell proliferation after treatment with BsGNPs, IgG-GNPs, free trastuzumab and pertuzumab, or a single-antibody cocktail of trastuzumab-conjugated GNPs and pertuzumab-conjugated GNPs (Ab-GNP cocktail), at the equivalent antibody dose of 3 μg/mL. BsGNPs significantly reduced SKBR3 cell proliferation compared to the other treatments. * $P < 0.05$, ** $P < 0.01$, **** $P < 0.0001$; one-way ANOVA with Tukey's post hoc. Data shown as percentage of the untreated control (mean ± SD of n=3 biological replicates; $n = 3$ technical replicates per biological replicate); (C) Cell proliferation in HER2-positive breast cancer cell lines BT-474 and SKBR3 relative to low HER2-expressing A431 cells after treatment with BsGNPs (at 3 μg/mL bound antibody; one-way ANOVA with Tukey's post hoc; * $P < 0.05$; mean ± SD of n=3 biological replicates, $n = 3$ technical replicates per biological replicate); (D) Cytotoxicity assays in HepG2 and KUP5 cells. Cells were treated with BsGNPs at gold concentrations of 10, 20, 50, or 100 μg/mL for 48 h, and viability was determined by MTT assay. Viability of BsGNP-treated groups was normalized to that of untreated control cells. No significant changes in viability were found (one-way ANOVA with Tukey's post hoc; mean ± SD of $n = 3$ biological replicates; $n = 3$ technical replicates per biological replicate). IgG-GNP: immunoglobulin G-conjugated gold nanoparticle; BsGNP:

bispecific gold nanoparticle; KUP5: Mouse Kupffer cell line; ANOVA: analysis of variance; SD: standard deviation; HepG2: human hepatocellular carcinoma cells.

increases with HER2 expression level. The absence of cytotoxicity in HepG2 and KUP5 cells further supports the favorable *in vitro* biocompatibility of the BsGNP platform.

In vivo antitumor efficacy of BsGNPs

We next evaluated the tumor targeting capacity and therapeutic efficacy of BsGNPs in a HER2-positive xenograft mouse model.

BT-474 cells were used due to their established ability to form robust HER2-overexpressing xenografts. Tumor-bearing nude mice were injected IP with either BsGNPs, a single antibody-GNP cocktail (trastuzumab-GNPs and pertuzumab-GNPs), or the combination of free trastuzumab and pertuzumab (all groups at equivalent antibody doses, weekly, over four weeks).

Intratumoral delivery of BsGNPs was evaluated by CT imaging at 24 h post-injection, demonstrating clear accumulation of the nanoparticles within the tumors [Figure 4A]. The single-antibody-GNP cocktail was also detectable within the tumors [Figure 4A]. Quantitative elemental analysis of tumors at this time point showed similar intratumoral gold accumulation for both BsGNPs and antibody-GNP cocktail treatments (4.19% ± 1.1 %ID/g tissue and 4.57 ± 1.85 %ID/g tissue) respectively; mean ± SD, n = 3), indicating similar tumor delivery efficiency.

Next, biodistribution analysis across major organs showed high accumulation of BsGNPs in the liver, consistent with typical clearance patterns for gold nanoparticles, and negligible amounts in the heart [Figure 4B].

Tumor growth was monitored over time following treatment initiation [Figure 4C]. Notably, despite comparable intratumoral gold accumulation between BsGNPs and the antibody-GNP cocktail, BsGNP-treated tumors showed a marked suppression of tumor growth, with near-complete elimination by the endpoint, and tumor size significantly reduced compared to all other groups (P < 0.05-0.001). In contrast, treatment with free antibodies and the antibody-GNP cocktail resulted in partial inhibition of tumor growth and remained significantly less effective than BsGNPs by the final time point.

Mean body weight of the BsGNP-treated mice remained stable during the treatment period and was comparable to the untreated, free antibody- and single-antibody cocktail-treated groups, with no evidence of treatment-associated weight loss [Figure 4D]. Moreover, blood chemistry analysis revealed no abnormalities in key markers of renal and hepatic function following BsGNP treatment. Creatinine, urea, ALT, AST, and ALP levels remained within established reference ranges for mice[41,42]. Measured levels were 0.185 ± 0.007 mg/dL (reference range: 0.1-0.4 mg/dL), 55.7 ± 8.4 mg/dL (28-76 mg/dL), 30.0 ± 3.7 U/L (22-296 U/L), 129.4 ± 12.9 U/L (38-361 U/L), and 228.4 ± 11.6 U/L (56-356 U/L), respectively (mean ± SD; n = 5). These findings suggest favorable systemic tolerability of BsGNPs.

Together, our results demonstrate that simultaneous presentation of trastuzumab and pertuzumab on a single nanoparticle significantly augments therapeutic efficacy while maintaining biocompatibility.

DISCUSSION

Bispecific antibodies represent a powerful therapeutic concept, yet straightforward engineering and efficacy in solid tumors remain an open challenges[43]. Here, we show that a nanotechnology-based approach, using gold nanoparticles as a modular scaffold, provides an effective strategy for bispecific targeting in solid tumor settings.

In HER2-positive breast cancer, trastuzumab and pertuzumab exert complementary mechanisms of action, in which trastuzumab primarily inhibits ligand-independent signaling, and pertuzumab prevents HER2 heterodimerization with other ErbB family members[44,45]. Building on the established clinical success of this antibody combination, we developed BsGNPs that co-display trastuzumab and pertuzumab on a single nanoparticle. This modular platform enables straightforward antibody conjugation while avoiding complex recombinant bispecific engineering. In HER2-positive breast cancer models

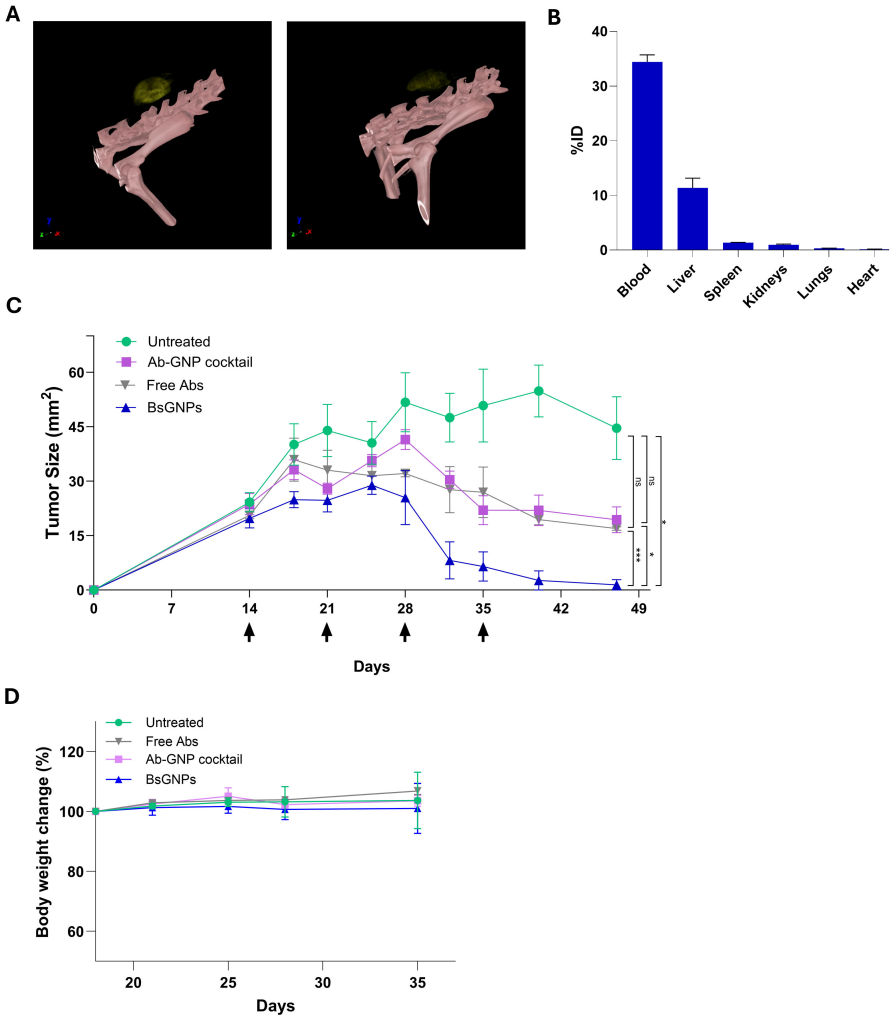

Figure 4. BsGNP treatment reduces tumor growth. (A) Representative micro-CT image of tumor-bearing mice at 24 h after BsGNP administration (left) or a cocktail of single-antibody GNPs (right) confirmed the intratumoral accumulation of the particles (golden-yellow colored); (B) Biodistribution profile of BsGNPs at 24 h post-administration, measured via ICP-OES; mean ± SEM, $n = 3$; (C) Tumor growth curves for untreated and treated with BsGNP, free antibodies, or the cocktail of antibody-GNPs. Arrows indicate treatment administration days. Results presented as mean ± SEM of $n = 5$ mice/group. *$P < 0.05$, *** $P < 0.001$, two-way ANOVA with repeated measurements followed by Tukey's multiple-comparisons test. Equivalent antibody doses (0.945 mg antibodies/injection) were given to free antibody-treated, cocktail-treated, and BsGNP-treated groups; (D) Body weight (% of baseline) in the untreated and treated groups measured during the treatment period. Data presented as mean ± SD of $n = 5$ mice/group. BsGNP: Bispecific gold nanoparticle; ID: injected dose; CT: computed tomography; ICP-OES: inductively coupled plasma optical emission spectrometry; SEM: standard error of the mean.

in vitro and *in vivo*, BsGNPs outperformed both the free trastuzumab-pertuzumab combination and a cocktail of trastuzumab-GNPs and pertuzumab-GNPs. Notably, tumor gold accumulation was comparable between BsGNPs and the single-antibody GNP cocktail, indicating that the enhanced efficacy of BsGNPs was not attributable to greater overall tumor delivery. One possible explanation is the close spatial co-presentation of trastuzumab and pertuzumab on the same nanoparticle. This arrangement may create a high local density of complementary binding specificities, thereby facilitating coordinated multivalent engagement of distinct HER2 epitopes and enhancing the cooperative activity of the two antibodies. Previous studies have shown that bispecific antibodies promote higher-order HER2 receptor clustering and enhance downstream signaling blockade[46,47]. Bispecific antibody nanoplatforms have also been reported to increase binding affinity and prolong receptor engagement[48,49]. Whether similar mechanisms contribute to the enhanced activity of BsGNPs remains to be determined in future studies.

In the clinic, dual HER2 blockade with trastuzumab and pertuzumab achieves its strongest antitumor activity when combined with chemotherapy[50],

whereas antibody-only regimens yield more modest responses[51]. Similarly, next-generation recombinant bispecific antibodies targeting HER2 epitopes have shown encouraging activity, yet their clinical benefit is often maximized in combination with chemotherapy. This underscores the need for strategies that could enhance the intrinsic efficacy of dual antibody-based targeting in solid tumors. BsGNPs represent a potential strategy to address this need by presenting intact antibodies in close proximity and enabling simultaneous arrival at the tumor, which could promote coordinated action upon tumor cells.

GNPs offer unique theranostic capabilities, serving both as CT contrast agents and therapeutic carriers. Their strong X-ray attenuation enables non-invasive, longitudinal tracking of drug delivery[23]. Thus, non-invasive CT imaging of BsGNPs can support image-guided therapy by monitoring delivery and assessing response at early time points, which is critical for optimizing treatment. We previously demonstrated that antibody-targeted GNPs allow tumor imaging and rapidly stratify responders versus non-responders, as early as 48 h post-treatment[21,22,27]. Thus, imaging with BsGNPs may select patients most likely to benefit from such therapy, enabling a more personalized, effective, and safer therapeutic approach. Such potential for stratification of responders will be evaluated in future studies.

Several limitations of the present study should be acknowledged. First, the molecular mechanisms underlying the enhanced activity of BsGNPs were not directly investigated. Approaches to assess the effects on receptor clustering, downstream signaling, and binding kinetics could help elucidate the mechanisms responsible for this enhanced activity. Second, the *in vivo* therapeutic efficacy was evaluated in a single HER2-positive xenograft model. Validation in additional tumor models, as well as evaluation of the platform with different antibody combinations targeting other tumor-associated biomarkers, will be important to establish its broader applicability. Finally, further studies evaluating the longitudinal biodistribution, clearance, and long-term safety of BsGNPs will be required for the continued development of this approach.

In summary, BsGNPs co-conjugating trastuzumab and pertuzumab represent a powerful and versatile platform that can overcome key limitations of conventional bispecific antibody therapies in solid tumors. By combining modular assembly, simultaneous antibody delivery, and theranostic capability, this strategy can promote nanoparticle-enabled bispecific therapies that are not only easier to engineer but potentially more effective in the clinic. Such platforms may ultimately redefine how multi-target antibody therapies are designed, delivered, and deployed in precision oncology.

DECLARATIONS

Authors' Contributions

Conceptualization: Popovtzer R, Fixler D
Design and supervision: Popovtzer R, Fixler D
Investigation: Anaki A, Tzror-Azankot C, Betzer O, Saidvaliev U, Zafran A, Motiei M
Data analysis: Anaki A, Tzror-Azankot C, Betzer O, Saidvaliev U, Zafran A and Sadan T
Writing - original draft: Anaki A
Writing - review and editing: Anaki A, Sadan T, Popovtzer R

Availability of data and materials

The data supporting the findings of this study are available from the corresponding author upon reasonable request.

AI and AI-assisted tools statement

During the preparation of this manuscript, the AI tool ChatGPT [OpenAI GPT-5.5 (released 2026-4-23) and GPT-5.6 (released 2026-07-09)] was used solely for language editing. The graphical abstract was generated using Google Gemini (Gemini 3.1 Flash Image, released 2026-02-26). The tools did not influence the study design, data collection, analysis, interpretation, or the scientific content of the work. All authors take full responsibility for the accuracy, integrity, and final content of the manuscript.

Financial support and sponsorship

This research was supported by the Israeli Ministry of Innovation, Science and Technology grant (no. 0008788) and the European Union ERC Consolidator Grant (no. 101044990). Views and opinions expressed are, however, those of the authors only and do not necessarily reflect those of the European Union or the European Research Council Executive Agency, and neither the European Union nor the granting authority can be

held responsible for them. This work was also supported by the Levtzion Scholarship granted to Anaki A by the Council for Higher Education of Israel.

Conflicts of interest

Betzer O is a co-founder and COO of Nanocarry Therapeutics Ltd. Popovtzer R is a co-founder and advisor of Nanocarry Therapeutics Ltd. Popovtzer R is an Associate Editor of *Nanomedicine Therapeutics*. Popovtzer R was not involved in any steps of editorial processing, notably including reviewers' selection, manuscript handling and decision making. The other authors declare that there are no conflicts of interest.

Ethical approval and consent to participate

The research was conducted in accordance with the guidelines and regulations of the National Institutes of Health according to the Guide for the Care and Use of Laboratory Animals, DHEW (NIH, Pub. 78-23). The Bar-Ilan University Institutional Animal Care and Use Committee approved the study protocol, and the study was conducted under its supervision (protocol no. 2401-104-5).

Consent for publication

Not applicable.

Copyright

REFERENCES

1. Klein C, Brinkmann U, Reichert JM, Kontermann RE. The present and future of bispecific antibodies for cancer therapy. *Nat Rev Drug Discov.* 2024;23:301-19. DOI PubMed
2. Guidi L, Etessami J, Valenza C, et al. Bispecific antibodies in hematologic and solid tumors: current landscape and therapeutic advances. *Am Soc Clin Oncol Educ Book.* 2025;45:e473148. DOI
3. Gu Y, Zhao Q. Clinical progresses and challenges of bispecific antibodies for the treatment of solid tumors. *Mol Diagn Ther.* 2024;28:669-702. DOI PubMed PMC
4. Shim H. Bispecific Antibodies and antibody-drug conjugates for cancer therapy: technological considerations. *Biomolecules.* 2020;10:360. DOI PubMed PMC
5. Iwasaki YW, Tharakaraman K, Subramanian V, et al. Generation of bispecific antibodies by structure-guided redesign of IgG constant regions. *Front Immunol.* 2022;13:1063002. DOI PubMed PMC
6. Madsen AV, Pedersen LE, Kristensen P, Goletz S. Design and engineering of bispecific antibodies: insights and practical considerations. *Front Bioeng Biotechnol.* 2024;12:1352014. DOI PubMed PMC
7. Baker JH, Lindquist KE, Huxham LA, Kyle AH, Sy JT, Minchinton AI. Direct visualization of heterogeneous extravascular distribution of trastuzumab in human epidermal growth factor receptor type 2 overexpressing xenografts. *Clin Cancer Res.* 2008;14:2171-9. DOI
8. Thurber GM, Schmidt MM, Wittrup KD. Antibody tumor penetration: transport opposed by systemic and antigen-mediated clearance. *Adv Drug Deliv Rev.* 2008;60:1421-34. DOI PubMed PMC
9. Bhatnagar S, Deschenes E, Liao J, Cilliers C, Thurber GM. Multichannel imaging to quantify four classes of pharmacokinetic distribution in tumors. *J Pharm Sci.* 2014;103:3276-86. DOI PubMed PMC
10. Rhoden JJ, Wittrup KD. Dose dependence of intratumoral perivascular distribution of monoclonal antibodies. *J Pharm Sci.* 2012;101:860-7. DOI PubMed PMC
11. Yu Y, Feng L, Liu Z. Nanomedicine sheds new light on cancer immunotherapy. *Med Rev (2021).* 2023;3:188-92. DOI PubMed PMC
12. Park JA, Wang L, Cheung NV. Modulating tumor infiltrating myeloid cells to enhance bispecific antibody-driven T cell infiltration and anti-tumor response. *J Hematol Oncol.* 2021;14:142. DOI PubMed PMC
13. Zhou S, Li F, Niu M, Wu K, Li T, Yi M. Advances in the clinical application of bispecific antibodies in cancer therapy. *iScience.* 2025;28:114203. DOI PubMed PMC
14. Mitchell MJ, Billingsley MM, Haley RM, Wechsler ME, Peppas NA, Langer R. Engineering precision nanoparticles for drug delivery. *Nat Rev Drug Discov.* 2021;20:101-24. DOI PubMed PMC
15. Li J, Yu X, Shi X, Shen M. Cancer nanomedicine based on polyethylenimine-mediated multifunctional nanosystems. *Prog Mater Sci.* 2022;124:100871. DOI
16. Wu JLY, Ji Q, Blackadar C, et al. The pathways for nanoparticle transport across tumour endothelium. *Nat Nanotechnol.* 2025;20:672-82. DOI
17. Wang B, Hu S, Teng Y, et al. Current advance of nanotechnology in diagnosis and treatment for malignant tumors. *Signal Transduct Target Ther.* 2024;9:200. DOI PubMed PMC
18. Anaki A, Tzror-Azankot C, Motiei M, Sadan T, Popovtzer R. Impact of synthesis methods on the functionality of antibody-conjugated gold nanoparticles for targeted therapy. *Nanoscale Adv.* 2024;6:5420-9. DOI PubMed PMC
19. Saha T, Fojtů M, Nagar AV, et al. Antibody nanoparticle conjugate-based targeted immunotherapy for non-small cell lung cancer. *Sci Adv.* 2024;10:eadi2046. DOI PubMed PMC

20. Zhang P, Rashidi A, Zhao J, et al. STING agonist-loaded, CD47/PD-L1-targeting nanoparticles potentiate antitumor immunity and radiotherapy for glioblastoma. *Nat Commun*. 2023;14:1610. DOI PubMed PMC
21. Reuveni T, Motiei M, Romman Z, Popovtzer A, Popovtzer R. Targeted gold nanoparticles enable molecular CT imaging of cancer: an *in vivo* study. *Int J Nanomedicine*. 2011;6:2859-64. DOI PubMed PMC
22. Dreifuss T, Betzer O, Shilo M, Popovtzer A, Motiei M, Popovtzer R. A challenge for theranostics: is the optimal particle for therapy also optimal for diagnostics? *Nanoscale*. 2015;7:15175-84. DOI
23. Bouché M, Hsu JC, Dong YC, Kim J, Taing K, Cormode DP. Recent advances in molecular imaging with gold nanoparticles. *Bioconjug Chem*. 2020;31:303-14. DOI PubMed PMC
24. Gao Q, Zhang J, Gao J, Zhang Z, Zhu H, Wang D. Gold Nanoparticles in Cancer Theranostics. *Front Bioeng Biotechnol*. 2021;9:647905. DOI PubMed PMC
25. Meir R, Popovtzer R. Cell tracking using gold nanoparticles and computed tomography imaging. *Wiley Interdiscip Rev Nanomed Nanobiotechnol*. 2018:10. DOI PubMed
26. Betzer O, Perets N, Angel A, et al. *In vivo* neuroimaging of exosomes using gold nanoparticles. *ACS Nano*. 2017;11:10883-93. DOI
27. Meir R, Shamalov K, Sadan T, et al. Fast image-guided stratification using anti-programmed death ligand 1 gold nanoparticles for cancer immunotherapy. *ACS Nano*. 2017;11:11127-34. DOI
28. Xi D, Dong S, Meng X, Lu Q, Meng L, Ye J. Gold nanoparticles as computerized tomography (CT) contrast agents. *RSC Adv*. 2012;2:12515. DOI
29. Liu X, Fang Y, Li Y, Li Y, Qi L, Wang X. Pertuzumab combined with trastuzumab compared to trastuzumab in the treatment of HER2-positive breast cancer: a systematic review and meta-analysis of randomized controlled trials. *Front Oncol*. 2022;12:894861. DOI PubMed PMC
30. Chen W, Yang L, Zhang J, Yuan Y. Efficacy of dual HER2 blockade in neoadjuvant HER2-positive breast cancer: a meta-analysis of RCTs. *Syst Rev*. 2026;15:45. DOI PubMed PMC
31. Jagosky M, Tan AR. Combination of pertuzumab and trastuzumab in the treatment of HER2-positive early breast cancer: a review of the emerging clinical data. *Breast Cancer (Dove Med Press)*. 2021;13:393-407. DOI PubMed PMC
32. Wang X, Lee KS, Zeng X, et al. Zanidatamab in combination with docetaxel in first-line HER2-positive breast cancer: results from an open-label, multicenter, phase Ib/II study. *ESMO Open*. 2025;10:105852. DOI PubMed PMC
33. Ma J, Wang J, Xu T, et al. Efficacy and safety of KN026 and docetaxel for HER2-positive breast cancer: a phase II clinical trial. *Cancer Commun (Lond)*. 2025;45:476-85. DOI PubMed PMC
34. Liu X, Fan X, Gao X, Hu W, Sun P. Leveraging HER2-targeted biparatopic antibodies in solid tumors. *Pharmacol Res*. 2025;214:107687. DOI
35. Zhang Q, Zhao W, Wang J, et al. Efficacy and safety results of TQB2930, a HER2-targeted bispecific antibody combined with chemotherapy in patients with HER2-positive breast cancer (BC) previously treated with ≥ 2 line treatments: results from a phase 1b/2 study. *JCO*. 2025;43:1033-1033. DOI
36. Enustun BV, Turkevich J. Coagulation of colloidal gold. *J Am Chem Soc*. 1963;85:3317-28. DOI
37. Ma T, Sun X, Cui L, et al. Molecular imaging reveals trastuzumab-induced epidermal growth factor receptor downregulation *in vivo*. *J Nucl Med*. 2014;55:1002-7. DOI
38. Björkelund H, Gedda L, Barta P, Malmqvist M, Andersson K. Gefitinib induces epidermal growth factor receptor dimers which alters the interaction characteristics with ^{125}I-EGF. *PLoS One*. 2011;6:e24739. DOI PubMed PMC
39. Maass KF, Kulkarni C, Betts AM, Wittrup KD. Determination of cellular processing rates for a trastuzumab-maytansinoid antibody-drug conjugate (ADC) highlights key parameters for ADC design. *AAPS J*. 2016;18:635-46. DOI PubMed PMC
40. Major M, Nervig CS, Gerland A, Owen SC. Surface-available HER2 levels alone are not indicative of cell response to HER2-targeted antibody-drug conjugate therapies. *Pharmaceutics*. 2024;16:752. DOI PubMed PMC
41. Quimby FW, Luong RH. Clinical chemistry of the laboratory mouse. In: The Mouse in Biomedical Research (Second Edition); Academic Press, 2006; pp 171-216. DOI PMC
42. Patel S, Patel S, Kotadiya A, et al. Comparative analysis of the effect of sex and age on the hematological and biochemical profile of BALB/c and C57BL/6 inbred mice. *J Am Assoc Lab Anim Sci*. 2025;64:132-45. DOI PubMed PMC
43. Lim K, Zhu XS, Zhou D, Ren S, Phipps A. Clinical pharmacology strategies for bispecific antibody development: learnings from FDA-approved bispecific antibodies in oncology. *Clin Pharmacol Ther*. 2024;116:315-27. DOI PubMed
44. Yamamoto Y. Overcoming trastuzumab-pertuzumab resistance and optimizing sequential anti-HER2 therapy in HER2-positive metastatic breast cancer. *Cancers (Basel)*. 2026;18:932. DOI PubMed PMC
45. Drittone D, Lucci C, Esposito L, Mazzuca F, Pisegna S. Impact of anti-HER2 therapies on overall survival in patients with HER2-positive metastatic breast cancer: focusing on intracranial efficacy of emerging treatments. *Cancers (Basel)*. 2025;17:3520. DOI PubMed PMC
46. Wang R, Jiang S, Zhang Q, Li J. The conditional promise of dual-epitope HER2 antibody-drug conjugates in breast cancer. *Cancer Biol Med*. ;2026:1-8. DOI
47. Herrera M, Pretelli G, Desai J, et al. Bispecific antibodies: advancing precision oncology. *Trends Cancer*. 2024;10:893-919. DOI

48. Duwa R, Choi J, Shrestha P, et al. Strengthened binding affinity of bispecific antibody nanoplatforms improved the anti-tumor efficacy. *Chem Eng J.* 2024;494:153128. DOI
49. Zheng J, Sun Y, Shen Y, Zhou Z. Surface engineering of nanoparticles for precision medicine. *Precis Med Eng.* 2025;2:100037. DOI
50. Kay C, Martínez-Pérez C, Meehan J, et al. Current trends in the treatment of HR+/HER2+ breast cancer. *Future Oncol.* 2021;17:1665-81. DOI
51. Huober J, Weder P, Veyret C, et al. PERNETTA: A non-comparative randomized open label phase II trial of pertuzumab (P) + trastuzumab (T) with or without chemotherapy both followed by T-DM1 in case of progression, in patients with HER2-positive metastatic breast cancer (MBC): (SAKK 22/10 / UNICANCER UC-0140/1207). *Ann Oncol.* 2018;29:viii93. DOI